Directed batch assembly of three-dimensional helical nanobelts through angular winding and electroplating

D J Bell[1]**, T E Bauert**[1]**, L Zhang**[1,2]**, L X Dong**[1]**, Y Sun**[3]**,
D Grützmacher**[2] **and B J Nelson**[1]

[1] Institute of Robotics and Intelligent Systems, ETH Zurich, CH-8092 Zurich, Switzerland
[2] Laboratory for Micro- and Nanotechnology, Paul Scherrer Institute, CH-5232 Villigen, Switzerland
[3] Advanced Micro and Nanosystems Laboratory, University of Toronto, M5S 3G8, Canada

E-mail: bnelson@ethz.ch

Abstract
This paper presents a new technique for the directed batch assembly of rolled-up three-dimensional helical nanobelts. The wet etch time is controlled in order for the loose end of the self-formed SiGe/Si/Cr nanobelts to be located over an electrode by taking advantage of the additional angular winding motion in the lateral direction. In a subsequent Au electroplating step, contacts are electroformed and the batch assembly is completed, while at the same time the conductance of the structures is increased.

(Some figures in this article are in colour only in the electronic version)

1. Introduction

Because of their interesting morphology, helical nanobelts can serve a variety of functions in micro- and nanoelectromechanical systems (MEMS and NEMS), such as springs, magnetic field detectors, chemical and biological sensors, electromagnets, and actuators. In the field of biomedical micro- and nanorobotics, nanocoils will enable wireless communication and energy transfer to untethered devices through inductive coupling. Compared to conventional planar induction coils, helical nanobelts minimize parasitic effects and allow further miniaturization. Many 3D helical structures with micro- and nano-features have been synthesized from different materials. Typical examples include carbon microcoils based on amorphous carbon [1], carbon nanocoils based on carbon nanotubes [2], amorphous boron carbide nanosprings [3], indium phosphide nanosprings [4], silicon carbide nanosprings [5], zinc sulfide nanobelts [6], and zinc oxide nanobelts [7, 8]. Liquid-based batch assembly developed on nanotubes [9], nanowires [10], and nanobelts [11] are likewise effective for integrating these structures into NEMS, though the yield will be low. On the other hand, a variety of other methods have been adopted to integrate larger helical microinductors into MEMS, such as polymer moulds [12–14], magnetic assembly [15], and stressed metal structures [16].

Recently, a new method of creating 3D helical structures with nanometre-scale dimensions has been presented [17]. The structures are created through a top-down fabrication process in which a strained nanometre thick heteroepitaxial bilayer curls up to form 3D structures with nanoscale features. Helical geometries and tubes with diameters between 10 nm and 10 μm can be achieved with good control over the electrical properties [18]. The experimental characterization of this type of structure has also been demonstrated previously [19, 20]. However, these structures have a fixed end and a free-standing end, which makes the assembly challenging [21]. Specially designed structures can have both ends bridged between electrodes, but the coil will have a dual-chirality. Robotic assembly is an option but is still a time-consuming process [22]. Based on an observation of the coil formation, we have developed a fabrication method that allows coils to assemble into a circuit by presetting electrode pads at the
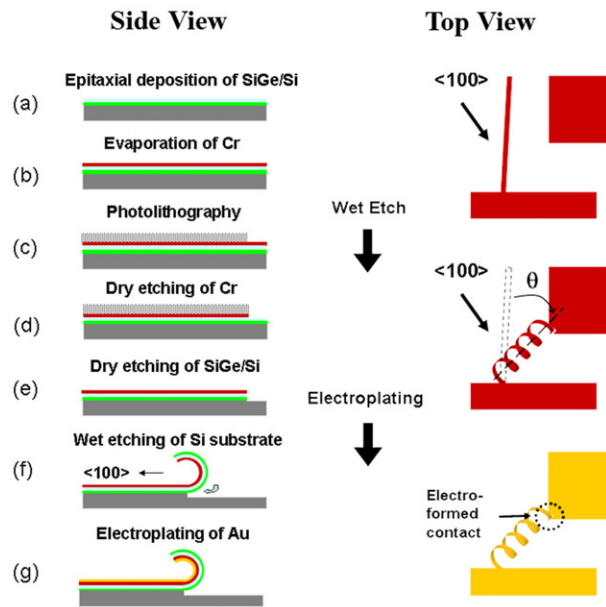
Figure 1. Process sequence: an initial planar bilayer patterned through conventional microfabrication techniques assembles itself into 3D nanostructures. This is achieved by controlling the wet etch time so that the loose ends of the nanobelts are located over electrode pads after scrolling. In a subsequent electroplating step, the loose ends are connected to the electrode pads.

free ends of the nanobelts and by electroforming contacts between them and the electrode pads. While the contacts are formed through electroplating, the conductance of these types of nanobelts is also increased. The process allows for the batch integration of nanobelts into NEMS and MEMS.

2. Fabrication

Figure 1 illustrates the fabrication process. One-side-polished $4''$ n-type Float Zone (100) Si wafers with high resistivity (10 kΩ cm) were used in order to minimize current leakage through the substrate. In the first part, 3D nanobelts were created that served as a frame for subsequent electroplating. For this purpose, a planar pattern was created in a heteroepitaxial $Si_{0.6}Ge_{0.4}$/Si bilayer with a Cr seed layer on top through conventional photolithography techniques and dry etching. The bilayers were grown by ultra-high vacuum chemical vapour deposition (UHV-CVD) at 550 °C (figure 1(a)). The thickness of the epi-grown layers was always smaller than the critical thickness to maintain elastic strain in the SiGe film [23]. For selectively etching the low-doped ($\sim 10^{14}$ cm^{-3}) Si substrate under the SiGe/Si heterostrucutres, the SiGe/Si bilayers were heavily boron doped (p+) to a level of 2×10^{20} cm^{-3}. An additional Cr layer was deposited by thermal evaporation on top of the bilayer (figure 1(b)). The initial pattern was created through photolithography with S1813 as a resist (figure 1(c)). After the development of the resist, the pattern was transferred into the Cr layer by Cl_2 and CO_2 plasma etching (figure 1(d)). Then RIE with a mixture of SF_6, CHF_3 and O_2 gases was used to transfer the pattern to the SiGe/Si bilayers at an etch rate of approximately 1 nm s^{-1} (figure 1(e)). After the dry etching, the wafers were diced into 15×10 mm^2 chips which were processed

separately for the remaining steps. For the self-scrolling of the nanostructures, samples were etched in 3.7% NH_4OH aqueous solution (figure 1(f)). The main advantages of NH_4OH–H_2O are that it does not incorporate alkaline ions which can contaminate CMOS integrated circuits, it is non-toxic, and it provides a higher selectivity to p + SiGe/Si bilayers (8000:1) than KOH [24]. During wet etching, the patterned bilayer curled up along the $\langle 100 \rangle$ direction releasing the internal strain and forming 3D structures. Then the samples were rinsed in deionized water and isopropyl alcohol and dried with a supercritical CO_2 dryer.

The fabrication method to this point is identical with what has been presented previously [20]. It results in nanobelts that are fixed on one side and have a loose end on the other side. However, in order to integrate them into an electrical circuit, it is necessary to have both ends connected. This is the focus of the work published in this paper. The self-scrolling process generates an additional angular winding motion in the lateral direction (θ in figure 1). The path of scrolling can, therefore, be predicted. By controlling the wet etch time, the final location of the released free end of the nanobelts can also be predicted. The masks are designed so that the released free end of the resulting nanobelt is located over an electrode pad so that a contact can be created between the nanobelt and the electrode pad after the wet etch release. The bridged nanobelt is then ready for the subsequent electroplating process. During the electroplating step, Au is deposited on the Cr seed layer. Where the initially loose end of a nanobelt is touching the underlying electrode pad, an electrical connection is electroformed. Cr was selected as a seed layer for electroplating due to good adhesion on silicon. The layer is 21 nm thick so that the resulting nanobelts have a sufficiently small radius of curvature. All of the structures and electrodes were initially connected to the same contact pad on one side of the chips. The connecting wires were long enough so that they could easily be broken after the electroplating for the electrical conductance measurements through the coils. An acid gold strike solution (Technic Inc., Acid Gold Strike) was identified to be suitable for electroplating onto this thin seed layer of Cr. The solution is based on potassium auric cyanid ($KAu(CN)_4$) and hydrochloric acid (HCl) diluted in water. The acid gold strike was kept in a plating bath which consisted of a bubble stirring device, a clamp for the chips and a clamp for the palladium anode. The clamps were connected to a DC power supply (American Reliance Inc., LPS-305) with a current range from 5 mA to 3 A. The setting for the optimum current to electroplate onto the Cr layer and the corresponding deposition rate and maximum thickness were determined with test chips with planar films. A current density of 1.4 mA cm^{-2} was found to give the best results with an almost linear deposition rate of 50 nm min^{-1}. It was achieved with the smallest possible current (5 mA) and additional copper foil connected to decrease the current density. After electroplating, it was not necessary to dry the structures in a supercritical CO_2 dryer, as they were strong enough to withstand surface tension forces due to the additional Au layer.

3. Results

Figure 2(a) shows a SiGe/Si/Cr nanobelt after the wet etch release step. The image was taken with a scanning electron

Figure 2. (a) SEM images of a released SiGe/Si/Cr nanobelt before electroplating. (b) Optical microscope image of a nanobelt after electroplating taken with a magnification of 100×.
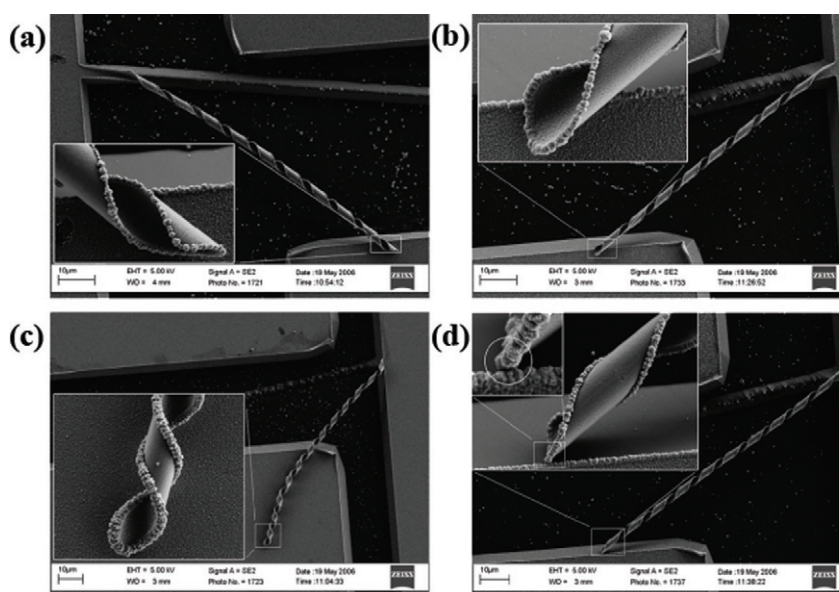

Figure 3. SEM images of SiGe/Si/Cr/Au nanobelts after electroplating. A right-hand coil (a) and a left-hand coil (b) make contact with the pre-fabricated electrodes. Coils make contact to the electrodes in two ways, at the corner (c) and on the surface (d) of the electrode pad.

microscope (SEM, Zeiss, ULTRA 55). Still visible in the right side of the image is the initial vertical strip pattern from which the coil formed. An electrode is designed according to the predicted angular winding displacement so that the nanobelt makes contact with it after the wet etch release. The etching time was controlled in order for the loose end of the coil to be positioned above the electrode after etching. The facets that evolve from the anisotropic wet etch are visible at the fixed end of the coil. The darker spots on the etched surface of the Si substrate are small etch pits where the wet etching propagated locally with the same characteristic facets evolving that evolve from the global etching. Scrolling is initiated at the tip of the strip pattern where it is first under-etched and then propagates towards the fixed end. A close-up image shows the thickness (41 nm) of the multilayer structure and the surface of the Cr layer that is used as a seed layer for subsequent electroplating. The roughness of this layer is low due to the epitaxial deposition of the SiGe/Si layer under the evaporated Cr layer.

During electroplating, an Au layer is grown on the Cr seed layer both inside the coil and on the electrodes. An electrical contact is electroformed between the initially loose end of the coils and the underlying electrodes. Cr was selected as a

seed layer for electroplating due to good adhesion on silicon. However, the layer is only 21 nm thick in order to ensure that the resulting nanobelts have a sufficiently small diameter. The setting for the optimum current to electroplate onto the Cr layer and the corresponding deposition rate and maximum thickness were determined with test chips with planar films. An optical microscope image (Leica, DM4000 M) of a typical sample after electroplating is shown in figure 2(b). Periodically, images such as this were obtained in order to monitor the results in the development of the process by observing the colour and texture of the electroplated surfaces as well as the shape and orientation of the coils. This also allowed for adjustment of the stirring intensity in the bath so that turbulence could be kept low enough in order for the coils not to become distorted. The coils had to remain over the electrodes underneath their loose ends so that the contacts could be electroformed.

For a more detailed investigation of the electroplated layers and electroformed contacts, SEM images were obtained after electroplating (figure 3). The electroplated Au layer can be recognized clearly in the images. The roughness of the Au layers is significantly larger than the roughness of the Cr layers that were evaporated on the epitaxial SiGe/Si bilayers. The
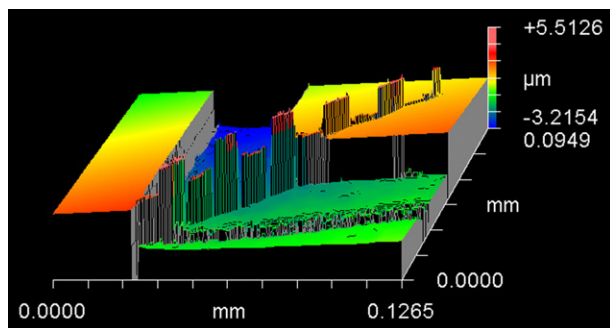
Figure 4. Result from the measurement with the white light interferometer.

Au surface looks similar on the electrodes and on the coils, indicating that the quality of the layer on the coils is similar to the large planar surfaces. Along the edges, the thickness of Au is larger than on surfaces and larger grains are visible. This is caused by voltage peaks that are generated in convex regions. The higher voltage causes the layer to grow faster which results in larger grains. Some Au was also electroplated a distance around the edge on the outer surface of the coils. In figure 3(d), the coil made contact with the electrode after scrolling from the side rather than from above. In the close-up image, a small electroformed contact is visible. The effective number of turns is smaller than the total number of turns of the nanobelts. Only the part of each nanobelt that is suspended over the gap between the electrodes is functional. The effective number of turns can be calculated by equation (1).

$$N_{\text{effective}} = \frac{g \tan \theta}{2 \pi R} \qquad (1)$$

where g is the gap between the two electrodes, θ is the angle as illustrated in figure 2, and R is the radius of curvature of the nanobelt.

Measurements of the thickness of the electroplated layers were performed with a white-light interferometer (Zygo, Newview 5022). In figure 4 a typical result is shown. Only surfaces near parallel to the substrate are visible because only these surfaces reflected the light back to the detectors. This is the case at the top and bottom of each turn of the nanobelts. The thickness of the electroplated Au layer was measured at the bottom of the turns where the coil is in contact with the underlying electrode. Average values for the thickness were taken over multiple areas.

All dimensions of the nanobelts after electroplating are summarized in table 1. The thickness of the SiGe/Si/Cr layers was approximately the same for all structures because all of the chips were made from the same wafer. A range is given for some parameters: for the diameter of the resulting structures there were some slight variations in the measurements. However, the diameter did not change during electroplating, indicating that the internal stress in the electroplated Au layers was low. The differences in pitch between turns for different coils are obtained by the differences in the orientation of the initial planar pattern. The number of turns varies with varying orientation and length of the pattern.

For electroplating, all structures and electrodes were connected to the same contact pad on the side of the chip.
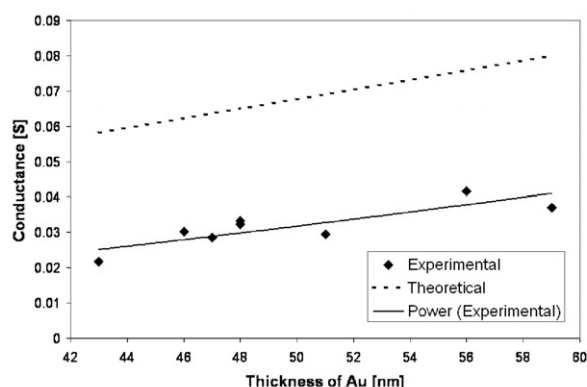

Figure 5. Plot of conductance versus measured thickness of the electroplated Au layer for different nanobelts. The dashed line indicates the theoretical conductance for a perfect Au layer with given thickness.

Table 1. Specifications of fabricated nanobelts.

Thickness $Si_{0.6}Ge_{0.4}$	12 nm
Thickness Si	8 nm
Thickness Cr	21 nm
Thickness Au	43–59 nm
Overall thickness	84–100 nm
Diameter	2.2–2.5 μm
Pitch	7–9 μm
Width of initial pattern	2–3.5 μm
Number of turns	5–9
Conductance	22–42 mS

There, the voltage was applied. After fabrication of the structures was completed, the wires that connected all the structures to the large pad on the side of the chip were broken so that the coils could be characterized individually. A probe station was used to contact the electrodes on both sides of the coils so that the electrical conductance through the coils could be measured with a multimeter. In order to verify that the contribution to the conductance from leakage currents through the substrate could be ignored, the conductance was also measured between electrodes with no coil connected. In figure 5, conductance is plotted versus the thickness of the electroplated Au layer. A power approximation is shown and compared with the theoretical prediction based on the expected value for a perfect layer of Au with the measured thickness and with the dimensions of the nanobelts. The results for the measured conductance are smaller than the theoretical conductance. This is because the electroplated layer does not have uniform thickness. Moreover, the electroformed contact is the cause of a further decrease in conductance. Its cross-sectional area is expected to be smaller than the cross-sectional area of the electroplated layer on the coils. This was clearly the case for the coil in figure 3(d). However, the results demonstrate that the electrical contacts are electroformed. Therefore, complete batch assembly is achieved, which allows for the integration of nanobelts through conventional silicon-based microfabrication techniques.

The fabrication process is suitable for further miniaturization. Nanometre-scale coil diameters can be achieved through changes in the layer design. Both the thickness of the layers

and the Ge content can be varied to change the resulting diameter. A smaller wire width can be obtained if the initial planar patterns are created through electron-beam lithography instead of photolithography, as illustrated in this paper. Also, the pitch between turns of the coils can be decreased. Two methods have been presented recently [25, 26]. For inductors, the smaller pitch can also result in a higher inductance.

4. Conclusions

The batch integration of helical nanobelts through conventional silicon-based microfabrication techniques was demonstrated. The wet etch time has been controlled in order for the loose end of the self-formed SiGe/Si/Cr nanobelts to be located over an electrode by taking advantage of the additional angular winding motion in the lateral direction. In a subsequent Au electroplating step, contacts have been electroformed and the batch assembly has been achieved, while at the same time the conductance of the structures is increased. The process represents an interesting extension to the field of the assembly of nanostructures. With existing techniques, such as dielectrophoretic self-assembly, chemically synthesized nanostructures self-assemble in liquid. However, with these types of methods, a high density of as-synthesized structures is needed in the liquid suspension, which is not compatible to as-fabricated nanostructures from conventional silicon-based fabrication techniques. In this paper, the fabrication and on-chip batch assembly of nanobelts have been integrated. With this process fewer structures are needed due to their higher yield for assembly. Furthermore, the geometry, location, and material properties of the as-fabricated structures can be controlled better than with as-synthesized nanostructures.

References

[1] Motojima S, Kawaguchi M, Nozaki K and Iwanaga H 1990 *Appl. Phys. Lett.* **56** 321–3

[2] Zhang X B, Zhang X F, Bernaerts D, Vantendeloo G T, Amelinckx S, Vanlanduyt J, Ivanov V, Nagy J B, Lambin P and Lucas A A 1994 *Europhys. Lett.* **27** 141–6

[3] McIlroy D N, Zhang D, Kranov Y and Norton M G 2001 *Appl. Phys. Lett.* **79** 1540–2

[4] Shen G Z, Bando Y, Zhi C Y, Yuan X L, Sekiguchi T and Golberg D 2006 *Appl. Phys. Lett.* **88** 243106-1–3

[5] Zhang D Q, Alkhateeb A, Han H M, Mahmood H, McIlroy D N and Norton M G 2003 *Nano Lett.* **3** 983–7

[6] Fang X S, Ye C H, Zhang L D, Wang Y H and Wu Y C 2005 *Adv. Funct. Mater.* **15** 63–8

[7] Kong X Y and Wang Z L 2003 *Nano Lett.* **3** 1625–31

[8] Xia Y N, Yang P D, Sun Y G, Wu Y Y, Mayers B, Gates B, Yin Y D, Kim F and Yan Y Q 2003 *Adv. Mater.* **15** 353–89

[9] Yamamoto K, Akita S and Nakayama Y 1996 *Japan. J. Appl. Phys.* 2 **35** L917–8

[10] Duan X F, Huang Y, Cui Y, Wang J F and Lieber C M 2001 *Nature* **409** 66–9

[11] Lao C S, Liu J, Gao P X, Zhang L Y, Davidovic D, Tummala R and Wang Z L 2006 *Nano Lett.* **6** 263–6

[12] Yoon Y K and Allen M G 2005 *J. Micromech. Microeng.* **15** 1317–26

[13] Yoon Y K, Park J W and Allen M G 2005 *J. Microelectromech. Syst.* **14** 886–94

[14] Chomnawang N, Lee J B and Davis W A 2003 *J. Microlith. Microfab.* **2** 275–81

[15] Zou J, Liu C, Trainor D R, Chen J, Schutt-Aine J E and Chapman P L 2003 *IEEE Trans. Microw. Theory Tech.* **51** 1067–75

[16] Chua C L, Fork D K, Van Schuylenbergh K and Lu J P 2003 *J. Microelectromech. Syst.* **12** 989–95

[17] Golod S V, Prinz V Y, Mashanov V I and Gutakovsky A K 2001 *Semicond. Sci. Technol.* **16** 181–5

[18] Golod S V, Grutzmacher D, David C, Deckardt E, Kirfel O, Mentese S and Ketterer B 2003 *Microelectron. Eng.* **67/68** 595–601

[19] Bell D J, Dong L X, Zhang L, Golling M, Nelson B J and Grützmacher D 2006 *Nano Lett.* **6** 725–9

[20] Bell D J, Sun Y, Zhang L, Dong L X, Nelson B J and Grützmacher D 2006 *Sensors Actuators* A **130/131** 54–61

[21] Cho A 2006 *Science* **313** 164–5

[22] Fukuda T, Arai F and Dong L X 2003 *Proc. IEEE* **91** 1803–18

[23] People R and Bean J C 1985 *Appl. Phys. Lett.* **47** 322–4

[24] Schnakenberg U, Benecke W and Lochel B 1990 *Sensors Actuators* A **23** 1031–5

[25] Zhang L, Ruh E, Grützmacher D, Dong L X, Bell D J, Nelson B J and Schönenberger C 2006 *Nano Lett.* **6** 1311–7

[26] Bell D J, Dong L X, Zhang L, Golling M, Nelson B J and Grützmacher D 2006 *Foundations of Nanoscience (FNANO) (Snowbird, UT)*